Gibson, V.B. et al. (2012) A novel method to allow noninvasive, longitudinal imaging of the murine immune system in vivo. Blood, 119 (11). pp. 2545-2551. ISSN 0006-4971

http://eprints.gla.ac.uk/62460

Deposited on: 17 December 2012

A novel method to allow noninvasive, longitudinal imaging of the murine immune system in vivo

Vivienne B. Gibson[*,1], **Robert A. Benson**[*,1], **Karen J. Bryson**[1], **Iain B. McInnes**[1], **Catherine M. Rush**[2], **Gianluca Grassia**[1,3], **Pasquale Maffia**[1,3], **Eric J. Jenkinson**[4], **Andrea J. White**[4], **Graham Anderson**[4], **James M. Brewer**[1], and **Paul Garside**[1]

[1]Institute of Infection, Immunity and Inflammation, College of Medical, Veterinary and Life Sciences, University of Glasgow, Glasgow, United Kingdom

[2]Microbiology and Immunology, School of Veterinary and Biomedical Science, James Cook University, Townsville, Australia

[3]Department of Experimental Pharmacology, University of Naples, Naples, Italy

[4]Medical Research Council Centre for Immune Regulation, School of Immunity and Infection, Medical School, University of Birmingham, Edgbaston, United Kingdom

Abstract

In vivo imaging has revolutionized understanding of the spatiotemporal complexity that subserves the generation of successful effector and regulatory immune responses. Until now, invasive surgery has been required for microscopic access to lymph nodes (LNs), making repeated imaging of the same animal impractical and potentially affecting lymphocyte behavior. To allow longitudinal in vivo imaging, we conceived the novel approach of transplanting LNs into the mouse ear pinna. Transplanted LNs maintain the structural and cellular organization of conventional secondary lymphoid organs. They participate in lymphocyte recirculation and exhibit the capacity to receive and respond to local antigenic challenge. The same LN could be repeatedly imaged through time without the requirement for surgical exposure, and the dynamic behavior of the cells within the transplanted LN could be characterized. Crucially, the use of blood vessels as fiducial markers also allowed precise re-registration of the same regions for longitudinal imaging. Thus, we provide the first demonstration of a method for repeated, noninvasive, in vivo imaging of lymphocyte behavior.

Correspondence: Paul Garside, Institute of Infection, Immunology and Inflammation, College of Medical, Veterinary and Life Sciences, Glasgow Biomedical Research Centre, University of Glasgow, 120 University Place, Glasgow, United Kingdom, G12 8TA; paul.garside@glasgow.ac.uk..
*V.B.G. and R.A.B. contributed equally to this study and should be considered joint first authors.

Introduction

Multiphoton laser scanning microscopy (MPLSM) has provided key insights into the kinetics and dynamics of the cellular interactions that govern the initiation of adaptive immune responses.[1-5] These studies have been performed ex vivo on excised lymph nodes (LNs) or in situ with surgically exposed LNs.[6] However, long-term imaging is limited by the effect of these procedures on the physiologic integrity of the LN, and longitudinal studies have been impractical.[1-5,7] We have therefore developed the novel approach of transplanting a LN into the murine ear pinna to facilitate in vivo MPLSM directly through the skin, allowing noninvasive, longitudinal imaging of cellular behavior in defined regions of the same LN.

Although previous studies have established the ear pinna as a site for transplantation of tissue such as spleen and heart,[8-12] the concept of transplanting a LN into the ear pinna of a mouse to facilitate imaging is entirely novel. Lymphoid tissue transfer has also long been accepted as a suitable method to study the development of lymphoid structures in vivo.[8,9,13] For example, the kidney capsule as a site of engraftment has proven invaluable for studying the development and organization of lymphoid tissue,[9,14] although relatively inaccessible for in vivo imaging. In this regard, LN transplantation into the ear pinna has a clear attraction. Here, we demonstrate that these transplanted LNs (tLNs) maintain the structural features, cellular organization, and functional capabilities of conventional LNs. Significantly, we show that tLNs have fully functional vascular and lymphatic supplies, allowing lymphocyte recirculation, Ag drainage by the afferent lymphatics, and levels of T-cell activation equivalent to those of normal LNs. Thus, our novel model provides a fully functional LN in an accessible location that allows previously impossible repeated and long-term in vivo MPLSM studies without surgical exposure/excision.

Methods

Animals

BALB/c (H-2^d), C57BL/6J (CD45.2, H-2^b), and Ly5.1/C57BL/6J (CD45.1, H-2^b) mice were used as recipients and donors. DO11.10 TCR transgenic (Tg) mice on a BALB/c background were used as a source of Ag-specific T cells for experiments that show the tLNs response to immunization.[15] These TCR Tg T cells recognize ovalbumin$_{323-339}$ in the context of I-A^d MHC-II and are detectable with the KJ1-26 clonotypic Ab. hCD2-GFP mice were used in MPLSM studies and express the green fluorescent protein (GFP) under the control of the human CD2 promoter, a cell surface molecule expressed on T cells.[16] All animals were specified pathogen free and maintained under standard animal house conditions at Strathclyde University or Glasgow University in accordance with Home Office Regulations.

Adoptive transfer of Ag-specific lymphocytes and in vivo challenge

Adoptive transfers were performed as described previously.[15] In some cases, cells were labeled with the fluorescent dye CFSE (Invitrogen) or Cell Tracker Red (CMTPX; Invitrogen) immediately before use.[15] Twenty-four hours after the adoptive transfer mice were challenged in the ear pinna with 50 μL of heat-aggregated ovalbumin or PBS as a control. Heat-aggregated ovalbumin was prepared as previously described[17] and was administered subcutaneously at a concentration of 100 μg/mouse. Cell Dark red fluorescent (660/680) 0.04-μm carboxylate-modified microspheres (FluoSpheres; Invitrogen) were used in LN transplantation experiments to show lymphatic drainage. PBS-diluted microbeads were injected subcutaneously into the outer edge of the ear pinna with tLNs.

Lymph node transplantation

Lymph nodes were removed from newly weaned 3- to 4-week-old mice, removing any excess fat, and placed into ice cold, sterile PBS (LNs were kept in this manner for no longer than 1 hour before transplantation). Whole LNs were inserted into a skin flap created in the ear pinna of the 8- to 12-week-old recipient. Veterinary-grade glue (Vetbond; 3M) was used to seal the skin flap. Successful grafts were identified visually (Figure 1A-B) and confirmed by soft tissue x-ray with the use of a Kodak FX Pro In-Vivo Imaging System (Carestream Health; Figure 1C). The tLNs were dissected for analysis after 3-4 weeks. For histologic studies, cervical, axillary or inguinal C57BL/6 donor LNs were engrafted to C57BL/6 recipients (all sources of LNs were able to produce viable tLNs, total replicates for this equals 11). To show repopulation of the tLN by recipient lymphocytes, CD45.1+ donor LNs were engrafted to CD45.2+ C57BL/6 recipients (n = 2 with 3 animals per group). For showing activation of Ag-specific T cells in the tLN, BALB/c donor LNs were engrafted to BALB/c recipients 3 weeks before adoptive transfer of DO11.10 TcR Tg T cells (n = 2). For in vivo multiphoton imaging studies, C57BL/6 donor cervical LNs were engrafted to the ear pinnae of hCD2-GFP recipients (n = 5).

Histopathology and immunofluorescence microscopy

Tissue samples in OCT embedding medium (Miles Diagnostic Division) were frozen in liquid nitrogen and stored at −70°C. Tissue sections (8 μm) were prepared on a cryostat (ThermoShandon) at −22°C. Sections were mounted onto SuperFrost slides (BHD) before being air-dried and stored at −20°C until further processing. H&E (Sigma-Aldrich) staining was performed on a Varistain 24-4 auto-staining processor (ThermoShandon). Tissue samples were then mounted in DPX mounting fluid (VWR International) before visualization by bright field microscopy. For fluorescence microscopy, tissue sections were stained with anti-CCL21–FITC, anti-VCAM-1–biotin, anti-CD3-biotin, anti-CD11c–FITC or biotin, anti-CD45.2–FITC, anti-CD4–FITC or pacific blue, anti-B220–FITC or biotin, anti-IgM–Rhodamine Red, anti-BP3–biotin, or anti-gp38–biotin. Streptavidin Alexa Fluor 647 (Invitrogen) or streptavidin-FITC (BD Biosciences) was used in conjunction with biotinylated primary Abs. Fluorescent images of the sections were captured with a Zeiss LSM 510 Meta confocal microscope equipped with a 20×/1.0NA water-immersion objective lens (Zeiss)

Flow cytometry

Flow cytometry was performed as described previously.[18] Abs or appropriately labeled isotype controls (anti-CD4–PerCP, anti-CD45.1–bio, anti-CD45.2–FITC, anti-CD8–APC, anti-B220–FITC, FITC-Mouse IgG2a isotype control, and FITC/PerCP/APC-rat IgG2a, κ isotype control; all BD Biosciences) and biotinylated KJ1.26 Ab) were added to each sample at a dilution of 1:100 Ab. Biotinylated Abs were detected by incubation with fluorochrome-conjugated streptavidin (BD Biosciences). Samples were analyzed with a FACSCanto flow cytometer equipped with a 488-nm Argon laser and a 635-nm red diode laser (BD Biosciences) and analyzed with FlowJo Version 9.4 software (TreeStar).

In vivo multiphoton imaging

Multiphoton imaging was performed with a Zeiss LSM7 MP system equipped with both a 10×/0.3 NA air and 20×/1.0NA water-immersion objective lens (Zeiss) and a tunable titanium/ sapphire solid-state 2-photon excitation source (Chameleon Ultra II; Coherent Laser Group). Excised LNs were bound with veterinary-grade glue (Vetbond; 3M) onto a plastic coverslip and adhered with grease to the bottom of the imaging chamber and continuously bathed in warmed (36.5°C), oxygenated CO_2-independent medium. For in vivo imaging, animals were anesthetized with fentanyl/ fluanisone (Hypnorm; Janssen Animal

Health) and (Hypnovel; Roche) injectable anesthesia (10 mL/kg of a mix of fentanyl/ fluanisone/midazolam/ H_2O at 1:1:2 by volume) given intraperitoneally. Core body temperature was continuously monitored and maintained by a thermostatically controlled heat mat. The ear of interest was mounted on a purpose-built stand with the use of veterinary-grade glue (Vetbond; 3M), enabling warming of tissue throughout the experiment and maintained at 37°C. At the end of imaging sessions, the veterinary glue was dissolved with 70% ethanol, allowing repeated imaging at a later date. Intravenous injection of nontargeted quantum dots (Qtracker 565 nontargeted quantum dots; Invitrogen) allowed highlighting of blood vessels. tLNs were routinely 100-150 μm from the ear surface, with images of cellular movement being made ~ 50 μm from the LN edge. Videos were acquired for 15-30 minutes at an X-Y pixel resolution 512×512 with 1.5-μm increments in Z. Three-dimensional tracking was performed with Volocity 5.5 (Perkin Elmer) after correction for tissue drift, and values representing the mean velocity, displacement, and meandering index were calculated for each object.

Statistics

Results are expressed as mean ± SD. Gaussian distribution was confirmed by D'Agostino and Pearson omnibus normality test before significance being determined by 2-way ANOVA. A value of *P*< .05 was regarded as significant.

Results

tLNs in the ear pinna are anatomically normal

Cervical, axillary, or inguinal C57BL/6J LNs from 3- to 4-week-old donors were engrafted to the ear pinna of 8-week-old syngeneic recipients. Donor LNs were inserted into small subdermal pockets on the ventral surface of the ear pinna. Mild, localized inflammation was observed at the transplantation site for 7 days after the procedure. By 3 weeks after transplantation, the superficial appearance of the ear pinna returned to normal, and the tLN/ site of engraftment was not obvious to the naked eye (Figure 1A). The tLN was visible within the lightly dissected pinnae and maintained its original size and shape (Figure 1B). By 3 weeks after transplantation, > 80% of the tLNs had engrafted and were readily identifiable in live mice with the use of soft tissue x-ray (Figure 1C). These tLNs were situated posterior to the auricular elastic cartilage and appeared histologically normal (Figure 1D).

Because the stromal cell network is essential for maintaining LN size and cellularity,[9] we examined the structural integrity of this compartment after the engraftment procedure. No marked differences were noted comparing control (non-tLN) with tLN for the distribution of BP-3 (Figure 2A), a glycosylated cell surface protein expressed by reticular stromal cells of secondary lymphoid tissue.[19] We also detected both donor and recipient CD45^{+}CD4^{+}CD3^{−} inducer cells in the tLN (supplemental Figure 1, available on the *Blood* Web site; see the Supplemental Materials link at the top of the online article), indicating that mechanisms known to be important in maintaining cellular organization and function in normal LNs are present in our tLN model.[20,21] Accordingly, conventional anatomic compartmentalization of T and B cells was evident in tLNs (Figure 2B). In addition, the overall proportion of CD4^{+}, CD8^{+} T cells and B220^{+} B cells was similar to control LNs (Figure 2C; supplemental Figure 2). CD11c staining showed normal distribution of dendritic cells throughout the paracortex (supplemental Figure 3). The conventional structural organization and cellular composition of tLNs indicates their capacity to support normal lymphocyte function, and a number of parameters were next examined to confirm this.

tLNs support lymphocyte recirculation

Lymphocyte recirculation is a crucial aspect of efficient immune surveillance.[22] Naive T and B cells enter LNs through high endothelial venules (HEVs). VCAM-1 is a key molecule that promotes adhesion of lymphocytes to the vascular wall of the HEVs[23] and was evident in tLNs (Figure 3A). HEVs are also a source of CCL21,[24,25] which actively recruits T cells to the paracortical area of the LN. CCL21 was present in control and tLN tissue sections, appearing throughout the T-cell area (Figure 3B). The presence of both HEVs and appropriate chemotactic cues implies that tLNs would indeed support lymphocyte recruitment.

To demonstrate this function, LNs were transplanted from C57BL/6J/CD45.1 mice into the ear pinnae of C57BL/6J/CD45.2 recipients. Three weeks after engraftment, tLNs had been repopulated with host CD45.2$^+$ T cells with 82.5% of lymphocytes with tLNs being CD45.2$^+$ (Figure 3C). The peripheral LNs from the recipient mouse were also pooled and analyzed for the presence of CD45.1$^+$ lymphocytes originating from the tLN. As might be expected very few CD45.1$^+$ cells could be detected, but a very small population was present (0.065%; Figure 3C). Thus, 3 weeks after transplantation, the tLN lymphocyte population predominantly consisted of CD45.2$^+$ lymphocytes. Normal recirculation by the tLN was also confirmed with the use of the adoptive transfer of fluorescently labeled lymphocytes (supplemental Figure 4).

Lymphatic drainage to the tLN

Afferent lymphatics are a critical component of immune surveillance, allowing LNs to selectively localize and trap Ag and APCs trafficked there from peripheral tissues. The presence of lymphatic vasculature supplying the tLN was assessed by examining the expression of gp-38, a cell surface glycoprotein preferentially expressed by stromal cells in T cell–dependent areas of secondary lymphoid organs and lymphatic endothelial cells.[26] Lymphatic vessels that express gp-38$^+$ were evenly distributed throughout the tissue and were associated with areas of CD4$^+$ staining in both control and tLN (supplemental Figure 5A-D), consistent with published reports of this glycoprotein being predominantly expressed in T-cell areas of the LN.[26] To directly examine the capacity of tLNs to drain material from its new anatomical location, fluorescent microbeads (0.04 μm) were injected into the tip of the ear pinna. Microbeads were easily detected in control, popliteal LNs after footpad injection (supplemental Figure 5E-F) and 24 hours later were localized within the CD4$^+$ T-cell area of the LN. Similarly, microbeads could be detected in the tLN (supplemental Figure 5G-H) after their injection into the tip of the ear pinna, confirming the ability of the transplant to form functional afferent lymphatics in its new tissue location.

tLNs support naive T-cell activation

We used adoptive transfer of CFSE-labeled TCR Tg T cells (DO11.10) to determine whether the tLN could facilitate activation of Ag-specific T-cell responses.[15] CFSE dilution and expansion of transferred cells was determined by flow cytometry 72 hours after immunization with Ag. The proportion of CD4$^+$KJ$^+$ cells in both the control and tLN was 4.82% and 4.78% respectively (Figure 4A-D) and was reflected in the loss of CFSE signal, indicative of cell division (Figure 4E-G). No difference in number of divisions between challenged control or tLNs was observed, indicating equivalent proliferative responses (summarized in Figure 4G). Overall, these data suggest that tLNs have a similar ability to control LNs in supporting Ag-driven lymphocyte activation and proliferation.

LN transplantation facilitates noninvasive, repeated imaging of dynamic lymphocyte behavior

C57BL/6 LNs were engrafted to hCD2-GFP mouse ear pinnae for longitudinal multiphoton imaging of GFP^{+} T cells in situ (Figure 5A-C; supplemental Videos 1-4). Recipient GFP^{+} T cells could be directly observed through the skin in the tLN without the requirement for surgical exposure, making longitudinal imaging feasible. Tracking studies found that lymphocytes in the tLN exhibited a significantly ($P < .001$) lower average track velocity ($4.21 \pm 2.3\ \mu m/min$) than those in excised popliteal LNs ($8.97 \pm 3.2\ \mu m/min$; Figure 5D; supplemental Figure 6A). Directional travel of T cells was found to be comparable between tLN and excised LNs with no significant difference in meandering index (Figure 5E; supplemental Figure 6B). A significant reduction in displacement rate of tLN T cells was also observed compared with excised LNs ($P < .001$; 1.80 ± 1.6 and $3.52 \pm 2.2\ \mu m/min$, respectively), probably reflecting the reduced velocity (Figure 5F; supplemental Figure 6C). Comparable track velocities between excised LNs and those surgically exposed and examined in situ have previously been reported. Although the T cells imaged in the tLNs behaved in a similar manner as those in an excised LN, they were somewhat slower. To replicate the effect of surgical exposure of LNs on T-cell behavior, we made small incisions adjacent to the tLNs under observation and then reimaged the original region 40 minutes later. A small increase in average track velocity (4.32 ± 2.1-$6.74 \pm 2.1\ \mu m/min$; $P < .001$) after tissue damage (Figure 5D; supplemental Figure 6A) was evident; however, this was still significantly lower than in excised LNs ($P < .001$). No significant alteration in meandering index was detected (Figure 5E); however, surgical intervention produced similar displacement rates to those seen in excised LNs (Figure 5F).

Because we did not have to perform surgery to permit imaging the tLN, we next sought to determine the potential of our model to reimage the same tissue at different time points. We chose to use blood vessels as fiduciary markers to guide reimaging of exactly the same region of the tLN. By injecting nontargeted quantum dots intravenously we were able to map blood vessels within the tLN during the initial imaging session. Injection of quantum dots also allowed us to visualize blood flow in vivo in the tLN, further indicating the successful formation of normal vasculature (Figure 6; supplemental Video 4). Importantly, mapping of blood vessels enabled us to re-register the imaging field to the same anatomical location in the tLN (Figure 7) as well as subsequently imaging lymphocyte behavior (supplemental Video 4 for day 1 and supplemental Video 5 for day 3). These findings emphasize the utility of this technique both for noninvasive repeat imaging in longitudinal studies and for imaging at a defined locus.

Discussion

Here, we describe a novel technique in which a LN is transplanted into the ear pinna of a mouse, providing a convenient anatomic location to facilitate in vivo MPLSM directly through the skin. This approach circumvents the requirement for the LN to be removed or surgically exposed and, significantly, has allowed the first longitudinal imaging of the same LN.

Established tLNs showed the key anatomic, cellular, and functional characteristics of control LNs. tLNs exhibited a normal stromal cell network, evidence of blood and lymphatic supply, and the presence of the chemokine CCL21, associated with coordinating localization of CD4^{+} T cells. CD45^{+}CD4^{+}CD3^{−} LN inducer cells of both host and donor origin were also detected within the tLN. These cells are known to play a critical role in LN development through their interactions with stromal organizer cells, which induces the release of chemokines and growth factors.[27] Furthermore, their continued presence in adult LNs is considered to be important in maintaining the organization of the LN. Presumably as

a result of all of this, the key cell types required for the initiation of an adaptive immune response, including T cells, B cells, and CD11c^{+} dendritic cells, were all detected in the usual proportions and locations in the tLN.

We also demonstrated the presence of vascular and lymphatic supplies to the tLN and that these were functional, capable of supporting lymphocyte recirculation and Ag drainage from tissue sites. Lymphocyte recirculation was evidenced by the presence of recipient T cells within tLN 3 weeks after transfer. Whether a tLN develops afferent lymphatic vessels capable of draining Ag from its new anatomic location had never been previously explored and was shown by injecting fluorescent microbeads into the peripheral tissue upstream of the tLN. Previous studies had indicated that neonatal spleens transplanted into the ear pinna were capable of responding to Ag challenge.[8] However, unlike LNs, spleens do not possess afferent and efferent lymphatic vessels, and the transplanted spleen was immunized directly with a targeted injection of Ag, thus, circumventing the requirement for tissue-draining lymphatic vessels.[8] Growth factors capable of directly inducing the growth of lymphatic vessels have been characterized and are up-regulated in response to environmental stress, including hypoxia, and can regenerate lymphatic vessels after tissue damage.[13] Therefore, the tLN system may also be useful in studying angiogenesis.

Flow cytometric analysis showed that immunization with ovalbumin in the ear pinna led to comparable Ag-specific T-cell proliferation in both the tLN and the control LN. This conclusively showed that the tLN is fully functional, undergoing vascularization to receive adoptively transferred T cells, draining Ag from a local injection site and supporting the cellular interactions required for clonal expansion of Ag-specific T cells. To confirm this final point, MPLSM was used to show T-lymphocyte movement within tLNs. Analysis of MPLSM data showed basically similar movement characteristics in tLNs and control LNs. Interestingly, lymphocytes in tLNs had reduced velocity and displacement rate compared with excised LNs, whereas sham surgery near the tLN increased these parameters. It is perhaps unsurprising that local trauma can affect lymphocyte function in draining LNs. Sterile trauma is known to promote inflammatory mediator release,[28] with dAMPs being important receptors in this process. In addition, localized tissue trauma increases lymphatic drainage, a process shown to increase intranodal levels of CCL21, potentially affected dynamic cellular migration patterns.[29] Our model avoids such effects that may complicate the interpretation of data according to approaches with explantation or exposure of LNs.

Importantly, because surgery was not required to image the tLNs, we also showed, for the first time, longitudinal imaging of the same LNs several days apart. For these studies, the ability to image the same tissue area was particularly important. To achieve this, we used blood vessels as fiduciary markers to re-register the imaging field to the same anatomic location in the tLNs during subsequent imaging sessions, clearly showing the potential of this technique for noninvasive, longitudinal imaging of cellular behavior.

In addition to visualizing spatially or temporally separated events, such as the physical movement of cells entering and leaving LNs, this approach opens up the potential for numerous other studies, including lymphangiogensis and vascularization; longitudinal imaging of infection, vaccinations, and tumors; and combining this technique with genetically modified animals to rapidly create compound transgenics.

In conclusion, we describe a new approach to imaging LNs in vivo with the use of MPLSM without the need for surgical exposure. This approach has allowed us to perform the first noninvasive, longitudinal imaging of lymphocyte behavior in vivo. We believe this model will provide a powerful tool to investigate a wide range of lymphocyte/lymphocyte and

lymphocyte/stromal cell interactions that regulate normal and pathologic immune responses in vivo and the effect of therapeutic intervention on these processes.

Supplementary Material

Refer to Web version on PubMed Central for supplementary material.

Acknowledgments

References

1. Stutzmann GE, Parker I. Dynamic multiphoton imaging: a live view from cells to systems. Physiology (Bethesda). 2005; 20:15–21. [PubMed: 15653835]

2. Celli S, Lemaitre F, Bousso P. Real-time manipulation of T cell-dendritic cell interactions in vivo reveals the importance of prolonged contacts for CD4+ T cell activation. Immunity. 2007; 27(4): 625–634. [PubMed: 17950004]

3. Schneider H, Downey J, Smith A, et al. Reversal of the TCR stop signal by CTLA-4. Science. 2006; 313(5795):1972–1975. [PubMed: 16931720]

4. Zinselmeyer BH, Dempster J, Gurney AM, et al. In situ characterization of CD4+ T cell behavior in mucosal and systemic lymphoid tissues during the induction of oral priming and tolerance. J Exp Med. 2005; 201(11):1815–1823. [PubMed: 15928201]

5. Itano AA, McSorley SJ, Reinhardt RL, et al. Distinct dendritic cell populations sequentially present antigen to CD4 T cells and stimulate different aspects of cell-mediated immunity. Immunity. 2003; 19(1):47–57. [PubMed: 12871638]

6. Sumen C, Mempel TR, Mazo IB, von Andrian UH. Intravital microscopy: visualizing immunity in context. Immunity. 2004; 21(3):315–329. [PubMed: 15357943]

7. Huang JH, Cardenas-Navia LI, Caldwell CC, et al. Requirements for T lymphocyte migration in explanted lymph nodes. J Immunol. 2007; 178(12):7747–7755. [PubMed: 17548612]

8. Cardillo F, Mengel J, Garcia SB, Cunha FQ. Mouse ear spleen grafts: a model for intrasplenic immunization with minute amounts of antigen. J Immunol Methods. 1995; 188(1):43–49. [PubMed: 8551037]

9. Carragher D, Johal R, Button A, et al. A stromaderived defect in NF-kappaB2-/- mice causes impaired lymph node development and lymphocyte recruitment. J Immunol. 2004; 173(4):2271–2279. [PubMed: 15294939]

10. Hillebrands JL, Klatter FA, Raue HP, Koops RA, Hylkema MN, Rozing J. An alternative model to study intrathymic tolerance induction: the neonatal heart-in-ear transplantation model in the rat. Transplant Proc. 1999; 31(3):1563–1566. [PubMed: 10331002]

11. Proudman S, Cleland L, Fusco M, Mayrhofer G. Accessible xenografts of human synovium in the subcutaneous tissues of the ears of SCID mice. Immunol Cell Biol. 1999; 77(2):109–120. [PubMed: 10234545]

12. Fulmer RI, Cramer AT, Liebelt RA, Liebelt AG. Transplantation of cardiac tissue into the mouse ear. Am J Anat. 1963; 113:273–285. [PubMed: 14061262]

13. Tammela T, Saaristo A, Holopainen T, et al. Therapeutic differentiation and maturation of lymphatic vessels after lymph node dissection and transplantation. Nat Med. 2007; 13(12):1458–1466. [PubMed: 18059280]

14. White A, Carragher D, Parnell S, et al. Lymphotoxin a-dependent and -independent signals regulate stromal organizer cell homeostasis during lymph node organogenesis. Blood. 2007; 110(6):1950–1959. [PubMed: 17526859]

15. Millington O, Di Lorenzo C, Phillips R, Garside P, Brewer J. Suppression of adaptive immunity to heterologous antigens during Plasmodium infection through hemozoin-induced failure of dendritic cell function. J Biol. 2006; 5(2):5. [PubMed: 16611373]

16. de Boer J, Williams A, Skavdis G, et al. Transgenic mice with hematopoietic and lymphoid specific expression of Cre. Eur J Immunol. 2003; 33(2):314–325. [PubMed: 12548562]

17. Leishman A, Garside P, Mowat A. Induction of oral tolerance in the primed immune system: influence of antigen persistence and adjuvant form. Cell Immunol. 2000; 202(2):71–78. [PubMed: 10896766]

18. Smith KM, Pottage L, Thomas ER, et al. Th1 and Th2 CD4+ T cells provide help for B cell clonal expansion and antibody synthesis in a similar manner in vivo. J Immunol. 2000; 165(6):3136–3144. [PubMed: 10975827]

19. McNagny KM, Bucy RP, Cooper MD. Reticular cells in peripheral lymphoid tissues express the phosphatidylinositol-linked BP-3 antigen. Eur J Immunol. 1991; 21(2):509–515. [PubMed: 1847877]

20. Yoshida H, Naito A, Inoue J, et al. Different cytokines induce surface lymphotoxin-alphabeta on IL-7 receptor-alpha cells that differentially engender lymph nodes and Peyer's patches. Immunity. 2002; 17(6):823–833. [PubMed: 12479827]

21. Luther SA, Ansel KM, Cyster JG. Overlapping roles of CXCL13, interleukin 7 receptor alpha, and CCR7 ligands in lymph node development. J Exp Med. 2003; 197(9):1191–1198. [PubMed: 12732660]

22. Butcher EC, Picker LJ. Lymphocyte homing and homeostasis. Science. 1996; 272(5258):60–66. [PubMed: 8600538]

23. Girard J, Springer T. High endothelial venules (HEVs): specialized endothelium for lymphocyte migration. Immunol Today. 1995; 16(9):449–457. [PubMed: 7546210]

24. Worbs T, Mempel TR, Bolter J, von Andrian UH, Forster R. CCR7 ligands stimulate the intranodal motility of T lymphocytes in vivo. J Exp Med. 2007; 204(3):489–495. [PubMed: 17325198]

25. Gunn MD, Tangemann K, Tam C, Cyster JG, Rosen SD, Williams LT. A chemokine expressed in lymphoid high endothelial venules promotes the adhesion and chemotaxis of naive T lymphocytes. Proc Natl Acad Sci U S A. 1998; 95(1):258–263. [PubMed: 9419363]

26. Farr AG, Berry ML, Kim A, Nelson AJ, Welch MP, Aruffo A. Characterization and cloning of a novel glycoprotein expressed by stromal cells in T-dependent areas of peripheral lymphoid tissues. J Exp Med. 1992; 176(5):1477–1482. [PubMed: 1402691]

27. Lane PJ, Gaspal FM, Kim MY. Two sides of a cellular coin: CD4(+)CD3- cells regulate memory responses and lymph-node organization. Nat Rev Immunol. 2005; 5(8):655–660. [PubMed: 16034364]

28. Kono H, Rock K. How dying cells alert the immune system to danger. Nat Rev Immunol. 2008; 8(4):279–289. [PubMed: 18340345]

29. Tomei A, Siegert S, Britschgi M, Luther S, Swartz M. Fluid flow regulates stromal cell organization and ccl21 expression in a tissueengineered lymph node microenvironment. J Immunol. 2009; 183(7):4273. [PubMed: 19734211]
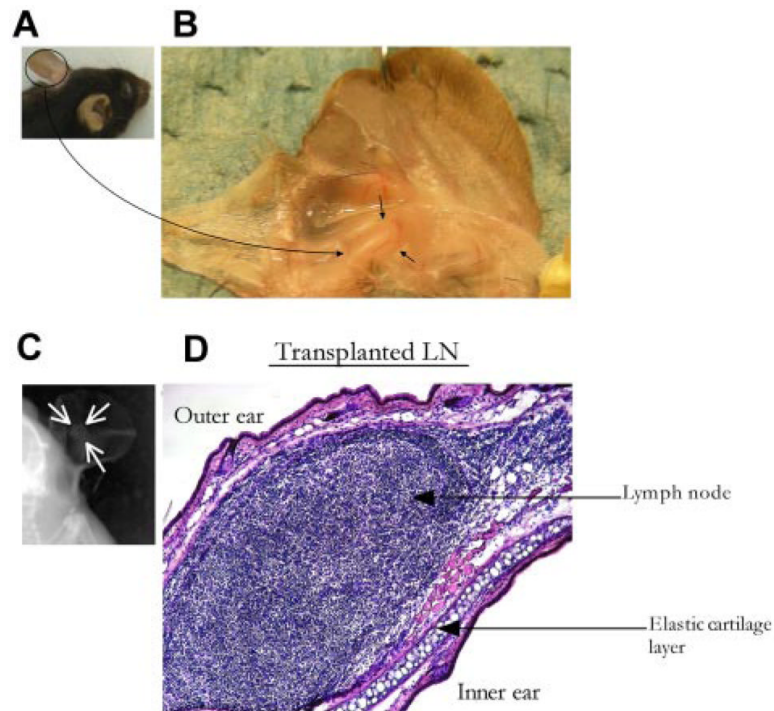
Figure 1. LN transplantation to the ear pinna
LNs from 4-week-old donor mice were inserted into subdermal pockets made in the ear pinna of adult C57BL/6 mice. The surgical incision was then sealed with veterinary-grade adhesive. Three to 4 weeks after engraftment, ear pinnae were harvested and sectioned for conventional histologic analysis. (A) Ear pinna before dissection. (B) Ear pinna containing the tLN, black arrows indicate the tLN surrounded by blood vessels. (C) Soft x-ray imaging identifies tLNs in ear pinna of live animals, marked by white arrows. (D) Ear pinna containing the tLN stained with H&E (magnification, ×10).
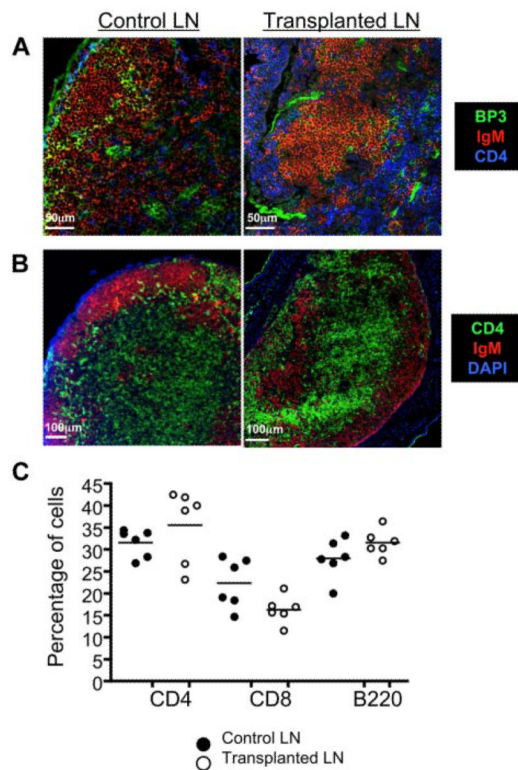
Figure 2. tLNs are anatomically normal

Three to 4 weeks after engraftment of syngenic LNs to C57BL/6 ear pinnae, tLNs were harvested and sectioned for immunofluorescent staining. (A) Confocal imaging of control and tLN showed equivalent BP3+ stromal cell (green) staining. CD4+ (blue) and IgM+ (red) staining allows T- and B-cell areas to be visualized for reference. Scale bars represent 50 µm. (B) Segregation of T cells and B cells was also evidenced by compartmentalization of CD4+ (green) T cell and IgM+ B cell (red) staining. Images shown are representative of 3 replicate mice; scale bars represent 100 µm. (C) tLNs were excised from the recipient animals, and single cell suspensions were made. Cells were then stained for B220, CD8, and CD4, and expression levels were determined by flow cytometry. These were compared directly to control, non-tLNs. The proportions of CD4+, CD8+T cells, and B220+ B cells in the tLN were found to be comparable with the control. Data show 6 replicate mice per group (see supplemental Figure 2 for representative plots and gating strategies).
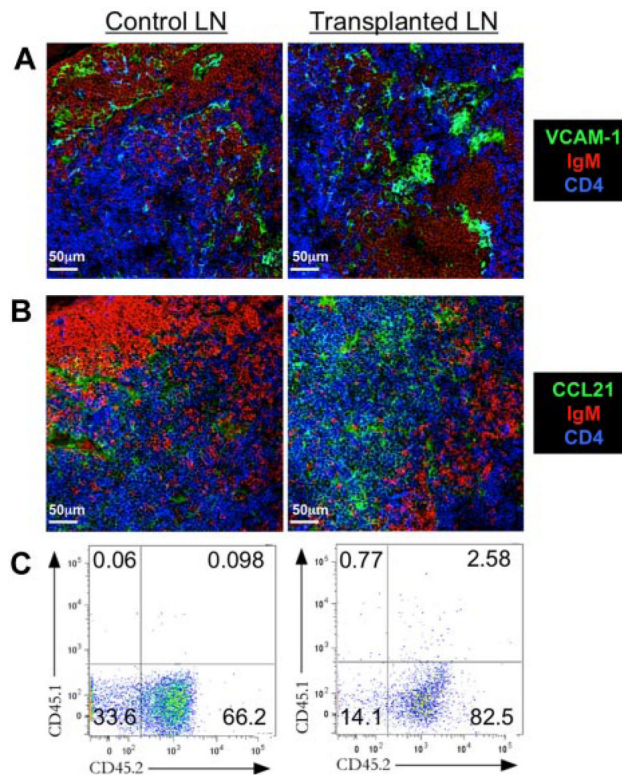
Figure 3. tLN supports lymphocyte recirculation
Three to 4 weeks after syngenic LN engraftment to C57BL/6 ear pinnae, tLNs and control LNs were harvested for sectioning and immunofluorescent staining. Control LNs and tLNs were compared for expression of the vascular endothelial cell marker (A) VCAM-1 (green) and (B) the chemokine CCL21 (green). Sections were also stained for $CD4^+$ cells (blue) and IgM^+ B cells (red). Images shown are representative of 3 replicate mice. To confirm recirculation, CD45.1 LNs were engrafted on CD45.2 recipients, and expression of CD45.1 and CD45.2 by control and tLN cells was assessed by flow cytometry. Scale bars denote 50 µm. (C) Representative flow cytometric plots show levels of CD45.1 and CD45.2 for both control and tLN.
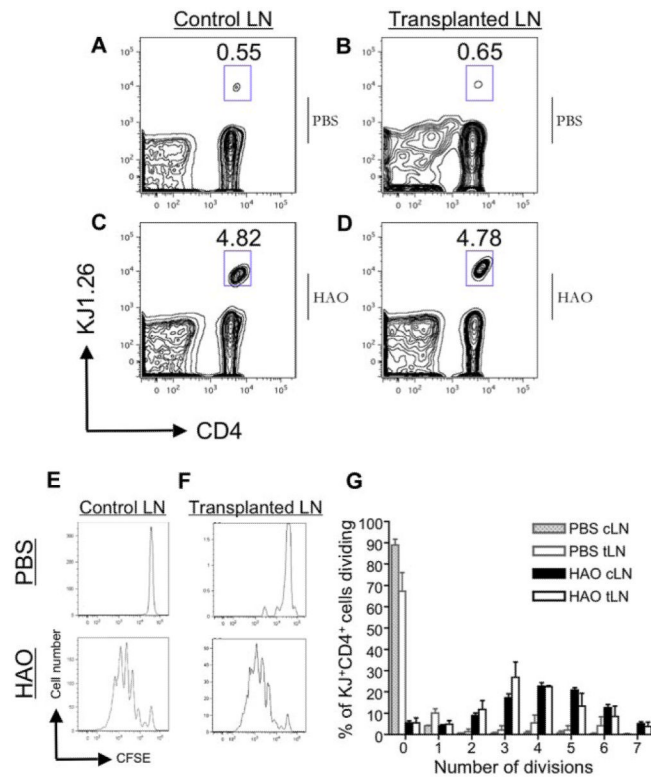
Figure 4. Activation of T cells in the tLN

Incremental loss of CFSE intensity by KJ1.26$^+$CD4$^+$ cells 72 hours after heat-aggregated ovalbumin (HAO) challenge in the ear showed proliferation of adoptively transferred DO11.10T cells in BALB/c mice with established tLNs. Representative flow cytometric plots of PBS-challenged cervical LN (A) and tLN (B). An expanded KJ1.26$^+$CD4$^+$ population is seen in both cervical (C) and tLN (D) after antigenic challenge. Incremental loss of CFSE intensity of KJ1.26$^+$CD4$^+$ cells in the cervical LN and tLN (E-F), reflecting Ag-specific proliferation that is summarized graphically (G). Data represent the mean of triplicate samples ± SD (n = 2).
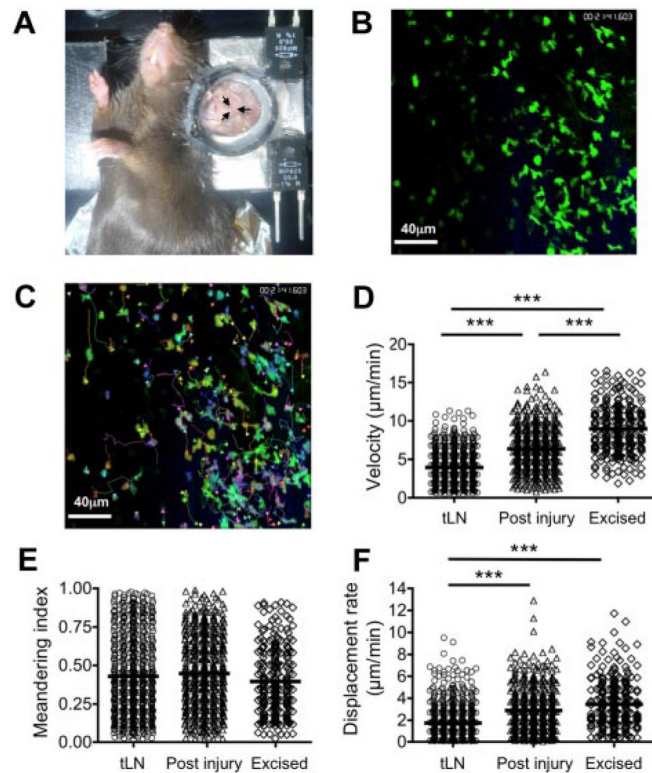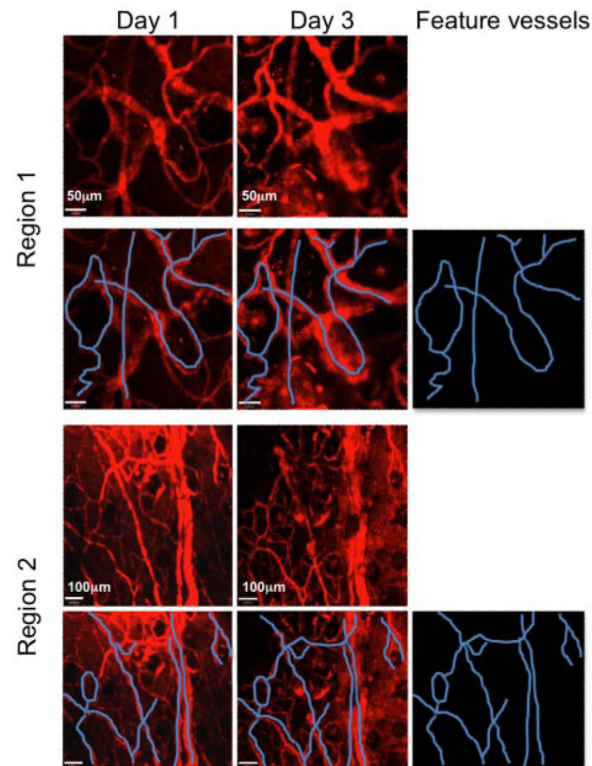
Figure 5. MPLSM of tLN

C57BL/6 LNs were engrafted to the ear pinnae of hCD2-GFP mice. Three to 4 weeks after engraftment, mice were anaesthetized, and the ear pinna was mounted on a heated stage (A). The tLN was then imaged by MPLSM without the need for surgical exposure (ie, through the intact ear). Recirculating GFP^{+} T cells in the tLN were imaged for 30 minutes (B), and cells were tracked (C) to allow calculation of velocity (D), meandering index (E), and displacement rate (F). After imaging the intact tLN, a surgical incision was made proximal to the engraftment area. After a period of 40 minutes, the tLN was imaged again, representing the LN after injury. Excised popliteal LNs from hCD2-GFP mice were imaged in a perfusion chamber as a control. Data represent tracks generated from 3 independent animals. Scale bars represent 40 μm. ***$P < .001$.
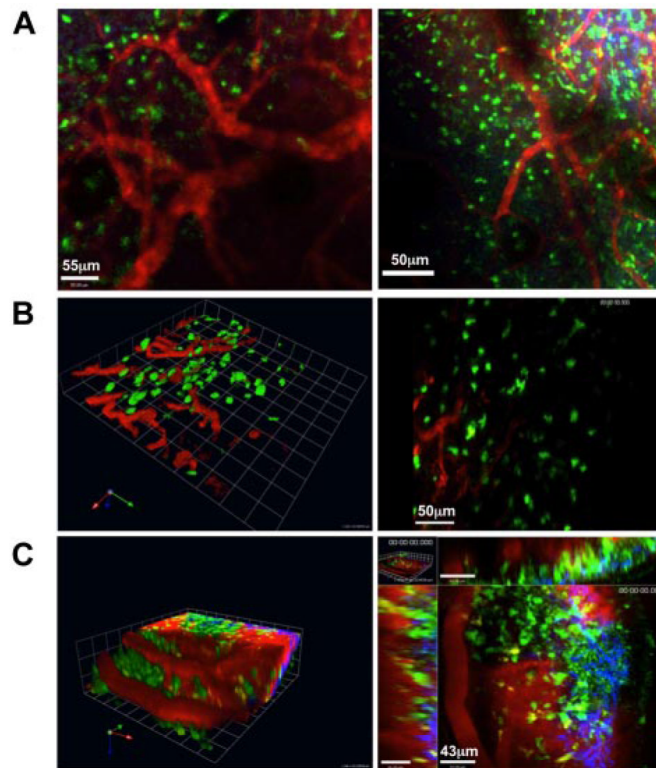
Figure 6. MPLSM of tLN
C57BL/6 LNs were engrafted to the ear pinnae of hCD2-GFP mice. Three to 4 weeks after engraftment, mice were anaesthetized, and the ear pinna was mounted on a heated stage. Vasculature throughout the tLN was clearly visible after intravenous injection of nontargeted Qdots (red); GFP$^+$ cells (green); second harmonic signal (blue). (A) Extended focus images of 60-μm z-stacks showing 2 different regions of the same tLN in left and right panels (scale bars, 55 μm and 50 μm, respectively). (B left panel) Three-dimensional reconstruction of blood vessels in the tLN. (B right) The corresponding extended focus image is shown; scale bar, 50 μm. (C left) Three-dimensional reconstruction of a third tLN showing vasculature. (C right) A representative optical section from the same z-stack is shown; scale bar, 43 μm. Images were acquired with a 20×/1.0NA water-immersion objective lens. Representative images from 3 independent animals are shown.

Figure 7. tLNs can be repeatedly imaged in the same area days apart
C57BL/6 LNs were engrafted to the ear pinnae of hCD2-GFP mice. Three to 4 weeks after engraftment, mice were anaesthetized, and the ear pinna was mounted on a heated stage. Vasculature was visualized with nontargeted Qdots (red). Several regions of the tLN were imaged where distinctive areas of vasculature were present. Two such areas are shown (Regions 1 and 2). Mice were then recovered and returned to the animal facility. Animals were then reimaged 3 days later. The same distinct areas of vasculature could be found in the naive tLN, confirming that the same area could be imaged longitudinally. Feature blood vessels are highlighted in blue. Scale bars in Region 1 images denote 50 μm. Scale bars in Region 2 images denote 100 μm. Images were acquired with a 10×/0.3NA air objective lens. Two representative regions are displayed from the same tLN.